Searching for correlations in simultaneous X-ray and UV emission in the narrow-line Seyfert 1 galaxy 1H 0707–495

D. R. S. Robertson,[1,2]★ L. C. Gallo,[1] A. Zoghbi[3] and A. C. Fabian[4]

[1]*Department of Astronomy and Physics, Saint Mary's University, 923 Robie Street, Halifax, NS B3H 3C3, Canada*
[2]*Department of Physics and Astronomy, McMaster University, Hamilton, ON L8S 4M1, Canada*
[3]*Department of Astronomy, University of Michigan, 1085 South University Avenue, Ann Arbor, MI 48109, USA*
[4]*Institute of Astronomy, University of Cambridge, Madingley Road, Cambridge CB3 0HA, UK*

ABSTRACT

We examine simultaneous X-ray and UV light curves from multi-epoch 8 d *XMM–Newton* observations of the narrow line Seyfert 1 galaxy 1H 0707–495. The simultaneous observations reveal that both X-ray and UV emission are variable and that the amplitude of the X-ray variations is significantly greater than that of the UV variations in both epochs. Using a discrete correlation function the X-ray and UV light curves were examined for correlation on time-scales up to 7 d. Low-significance ($\sim$95 per cent confidence) correlations with the UV leading the X-ray variations are observed. The lack of a significant correlation between the UV and X-ray bands seems consistent with the X-ray source being centrally compact and dominated by light bending close to the black hole. In addition, multiband X-ray light curves were examined for correlations on similar time-scales. Highly significant ($>$99.9 per cent confidence) correlations were observed at zero lag consistent with previous studies of this active galactic nucleus.

Key words: galaxies: active – galaxies: individual: 1H 0707–495 – galaxies: Seyfert – X-rays: galaxies – X-rays: individual: 1H 0707–495.

1 INTRODUCTION

Active galactic nuclei (AGNs) are characterized by their broad spectral energy distribution (SED) that extends over all observable wavelengths. In the standard paradigm, the UV emission is attributed to thermal emission from the accretion disc, while the X-rays originate from Comptonization of UV disc photons in a centrally compact corona of relativistic electrons. While the emitting regions may be physically distinct, interplay between them is predicted. If the corona indeed creates X-ray emission through Comptonization of disc photons, then one would expect that variations seen in the UV emission would propagate into the X-ray producing corona after some time delay. Similarly, some X-ray photons emitted by the corona will inevitably illuminate the accretion disc where they will be reprocessed and seen in the UV. Variability in X-ray will then be echoed in UV at a later time corresponding to light-travel time between the regions if the reprocessing time-scales are negligible.

The search for correlation between UV and X-ray emission has generated mixed results. Smith & Vaughan (2007, hereafter SV07) examined a sample of 10 Seyfert 1 galaxies with simultaneous X-ray and UV data obtained with *XMM–Newton* using a discrete correlation function (DCF; Edelson & Krolik 1988). Their work was

mainly sensitive to short time-scale correlations, less than $\sim$2 d. SV07 found only one object, NGC 4051, that exhibited a modestly significant lag ($\sim$68–95 per cent confidence), with the X-ray leading the UV by about 0.2 d. These findings corroborated earlier conclusions by Mason et al. (2002), which found a similar 0.2 d lag in NGC 4051 with $\sim$85 per cent confidence. On the other hand, SV07 refute a 1.6 d lag (UV leading X-ray) in MCG–6–30–15 that was earlier reported by Arèvalo et al. (2005).

Further work on NGC 4051 utilizing 15 *XMM–Newton* observations over 45 d revealed the UV lagging X-ray by $\sim$3 ks (Alston, Vaughan & Uttley 2013). Alston et al. (2013) find the lag is consistent with thermal reprocessing of X-rays. Breedt et al. (2010) examined NGC 4051 on longer time-scales using 12 years of monitoring data and find two significant correlated peaks at $\sim$1.2 and 39 d. In both cases, the X-ray lead the UV variations also suggesting X-ray reprocessing in the disc and torus. However, Alston et al. (2013) did not find any significant correlations on similar time-scales.

Cameron et al. (2012) examined one of the smallest known supermassive black holes, NGC 4395, using *Swift*. Over the course of a year from 2008 April to 2009 March, Cameron et al. (2012) collected data in the *UVW*2 filter (212 nm rest frame) and X-ray (2–10 keV) to probe long-term variability between the wavebands. Using a cross-correlation function (CCF) Cameron et al. (2012) were able to determine a correlation of zero lag between the UV

★E-mail: roberd9@mcmaster.ca

Table 1. *XMM–Newton* observation log for 1H 0707–495. The * denotes X-ray observations affected by high radiation.

Rev.	Observation ID	Start date (UTC)	Duration (s)	UV filter	UV exposures	UV exposure length (s)
1491	0511580101	2008/01/29 18:10:59	121 591	*UVW*1	72	1200
1492*	0511580201	2008/01/31 18:03:18	105 713	*UVW*1	75	1200
1493*	0511580301	2008/02/02 17:55:35	104 157	*UVW*1	75	1200
1494*	0511580401	2008/02/04 17:57:46	101 785	*UVW*1	75	1200
1971*	0653510301	2010/09/13 00:14:45	128 467	*UVW*1	0	–
1972*	0653510401	2010/09/15 00:16:54	127 867	*UVW*1	15	4400
1973*	0653510501	2010/09/17 00:19:15	127 268	*UVW*1	13	4400
1974*	0653510601	2010/09/19 00:18:10	126 867	*UVW*1	13	4400

and X-ray regimes, only when rebinning did they find a lag of 0.005 d with 99 per cent confidence over ±40 d.

Other works examining various time-scales have found evidence for UV leading X-ray (e.g. Shemmer et al. 2003; Marshall, Ryle & Miller 2008), X-ray leading UV (Nandra et al. 1998; Shemmer et al. 2001, Breedt et al. 2010; Lohfink et al. 2014), and significantly correlated light curves with zero lags (e.g. Breedt et al. 2009). While in theory an examination for correlations would appear straightforward, in practice there are several challenges related to data sampling, inconsistencies between instruments, and the different variability behaviour exhibited in the X-ray and UV (e.g. not all features seen in one band are necessarily manifested in the other). In general, the UV/X-ray mechanism is more complicated than originally thought and more work with high-quality, well-sampled data is required.

One of the best-studied AGN with *XMM–Newton* is the narrow-line Seyfert 1 galaxy (NLS1), 1H 0707–495. Noted for its extreme X-ray variability (e.g. Gallo et al. 2004) and complex spectra (e.g. Boller et al. 2002; Fabian et al. 2002, 2004, 2012), 1H 0707–495 was the subject of two very deep 500 ks pointed observations in 2008 and 2010. The 2008 observations resulted in the discovery of relativistically blurred Fe Lα (Fabian et al. 2012) and a reverberation lag of 30 and 200 s between the primary power law and blurred reflection component (Fabian et al. 2012; Zoghbi et al. 2010).

The Optical Monitor (OM; Mason et al. 2001) functioned during both 2008 and 2010 observation epochs providing optical/UV simultaneously with X-ray data. These multiwavelength data have been used to study variability and the UV to X-ray SED in 1H 0707–495 (e.g. Gallo 2006; Vasudevan et al. 2011). The 2008 and 2010 deep observations are of particular interest for examination of correlated short-term UV/X-ray variability since the long observations of 1H 0707–495 were gathered predominantly with only one OM filter creating an uninterrupted UV light curve. For this reason, these data are the subject of this study. In this work, we examine the 2008 and 2010 deep observations of 1H 0707–495 for correlated UV and X-ray variability. In the following section we describe the observations and generated light curves. In Section 3, we describe the DCF method employed in this work and present our results. We discuss our results in Section 4 and provide concluding remarks in Section 5.

2 OBSERVATIONS, DATA REDUCTION, AND LIGHT CURVES

1H 0707–495 has been observed on 15 occasions with *XMM–Newton*. In this analysis, we are primarily interested with two sets of four consecutive observations conducted between 2008 January 29 and February 6 and 2010 September 13 and 21. During the 2008

epoch, the OM operated in imaging mode with the *UVW*1 (291 nm effective wavelength) filter in place for the entire duration. The 2010 epoch operated with the OM cycling through seven optical to UV filters; however, only data from the *UVW*1 filter are used. Data from these two epochs represent the longest observations of 1H 0707–495 in which UV and X-ray emission were observed (Table 1).

The *XMM–Newton* observation data files (ODFs) from each observation were processed to produce calibrated event lists using the *XMM–Newton* Science Analysis System (SAS v13.5.0). X-ray light curves were extracted from these event lists to search for periods of high background flaring and such periods have been neglected. Pile-up was negligible during the observations. The background photons were extracted from an off-source region on the same CCD close to the source. Single and double events were selected for the pn detector. For simplicity only the pn data are used here. The MOS data were determined to be completely consistent with the pn data by Zoghbi et al. (2010). X-ray data were divided into three energy bands: a low-energy (i.e. 'blackbody') band (0.3–0.5 keV; XRB), a soft band (0.5–1.0 keV; XRS), and an intermediate X-ray band (1.0–4.0 keV; XRI). The band selections correspond with the regions of interest identified by the spectral analysis of Zoghbi et al. (2010), where the intermediate band (XRI) is dominated by the direct power-law component and the soft band (XRS) is reflection dominated. The lowest energy band (XRB) is thought to have significant contribution from the accretion disc and it would be interesting to examine its relation with the UV variability.

UV light curves are generated from the `omichain` pipeline using SAS v13.5.0. Each UV exposure in the 2008 epoch had an exposure time of 1200 s that is set by the ODFs with a total of 297 exposures (Fig. 1). The UV count rate and count-rate error are extracted from the individual OM exposures and the time associated with each reading is assigned as the mid-point time for the exposure. Although exposure times are set at 1200 s, the actual time between UV data points is ~1500 s because each exposure was separated by a varying amount of time, usually ~300 s. UV images in the 2010 epoch had exposure times of 4400 s, with time between exposures varying. The exposure times and delays are intrinsic to the UV data collection process set by the ODFs. The source extraction region was much larger than the host galaxy in the UV. The host galaxy contamination was not accounted for, although its contribution is likely small (e.g. Leighly & Moore 2004; Vasudevan et al. 2011). In any event, the true amplitude of the UV variations from the AGN may appear smaller than it is intrinsically.

A second faint UV source located on the same CCD but outside of the 1H 0707–495 extraction region was found and a light curve was extracted in the manor described above. To probe for any systemic effects, a Pearson correlation coefficient was calculated between 1H 0707–495 and the secondary source. Both UV light curves were found to be completely uncorrelated ($\rho = -0.04$).
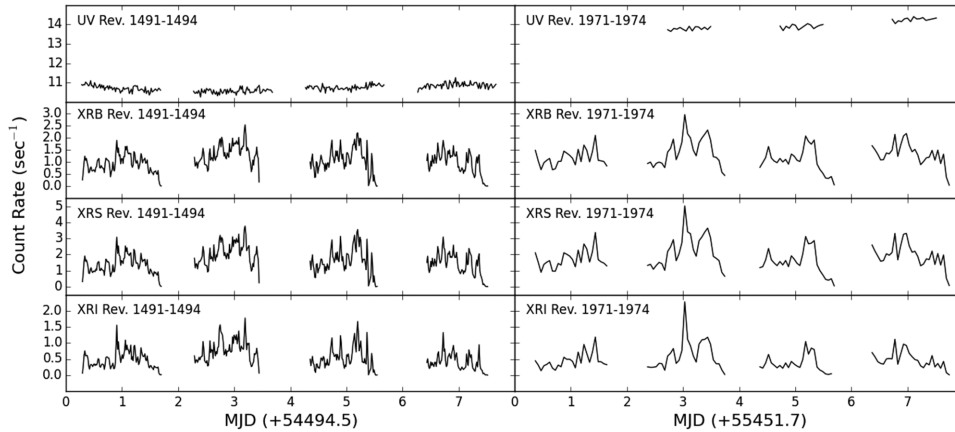
Figure 1. 1H 0707–495 UV (*UVW*1) and X-ray light curves at both epochs, Rev. 1491–1494 (left-hand panel) and Rev. 1971–1974 (right-hand panel). Errors in count rate are too small to be seen.

Table 2. Sampling and variability characteristics of UV and X-ray light curves. The epoch and energy band are given in Columns 1 and 2, respectively. Columns 3 and 4 describe the number of data points and the fractional variability in each light curve, respectively. The final column is the reduced χ^2 of a linear fit to the light curve.

Epoch	Light curve	N	F_{var}	χ_r^2
2008	UV (*UVW*1)	297	0.014	17.9
	XRB (0.3–0.5 keV)	349	0.852	937.0
	XRS (0.5–1.0 keV)	350	0.860	1360.3
	XRI (1.0–4.0 keV)	349	0.911	432.7
2010	UV (*UVW*1)	41	0.008	30.1
	XRB (0.3–0.5 keV)	109	0.427	1698.8
	XRS (0.5–1.0 keV)	108	0.492	2794.9
	XRI (1.0–4.0 keV)	109	0.621	798.0

To quantify the AGN variability in each light curve, we calculate the fractional variability (F_{var}; Markowitz, Edelson & Vaughan 2003) and the reduced, χ_r^2, to a linear model (Table 2). The amplitude of the UV variations are notably less than in the X-rays, none the less they are significant. The two epochs were examined separately for correlations between the light curves and found to be consistent. The analysis presented here is for the combined 2008 and 2010 data sets. X-ray light curves were generated in each band and were binned in time to match the exposure length of the respective UV light curves. By construction, the X-ray light curves were binned uniformly with data points every 1200 s in the 2008 epoch and 4400 s in the 2010 epoch. The UV light curves are unevenly sampled with a non-uniform separation in time which is set by the OM exposures.

Vasudevan et al. (2011) fitted the UV to X-ray SED for 1H 0707–495 with a simple multicolour blackbody accretion disc and a broken power-law model. The maximum disc temperature estimated from the SED fit was between 45 and 50 eV. Assuming a geometrically thin, optically thick accretion disc the emission originates from approximately $20\,R_S$ ($1R_S = 2GM/c^2$) if the AGN is accreting at the Eddington rate.

The disc emission associated with the *UVW*1 filter is significantly redwards of the peak disc emission and the flux density is less than about 1/50 the flux density at the peak (Vasudevan et al. 2011). We can estimate the expected time delay by considering the distance at which the *UVW*1 radiation is emitted from in the disc. Assuming a

geometrically thin, optically thick accretion disc with no additional sources of heating (e.g. X-ray illumination) and using Wien's Law to estimate temperature, the distance is

$$\frac{r}{R_S} = \left[\left(\frac{\dot{M}}{\dot{M}_E} \right)^{-1/4} \frac{M_{bh}^{1/4}}{6.3 \times 10^7} \frac{b}{\lambda} \right]^{-4/3}, \tag{1}$$

where $\dot{M}/\dot{M}_E$ is the Eddington mass accretion rate, M_{bh} is black hole mass in units of solar mass and $b = 0.0029$ (Peterson 1997). If we consider a range of $\dot{M}/\dot{M}_E = 0.01$-1, where higher values are likely more representative of NLS1s like 1H 0707–495, and adopt a black hole mass of $M_{bh} = 2 \times 10^6\,M_\odot$ (Tanaka et al. 2004), the *UVW*1 radiation is emitted from a radius of $r \approx 200$–$900\,R_S$ from the black hole, which is ∼10–50 times farther than where the peak disc emission originates from. The scale corresponds to a light-travel time that is ∼0.05–0.23 d from the central black hole.

Distances could be larger if, for example, X-ray heating were important. We also note that the small amplitude of the *UVW*1 variations (∼1 per cent, Table 2) indicate that only a small fraction of the entire *UVW*1-emitting region need be producing the fluctuations. In any event, light-travel time effects of this order should be measurable given the timing resolution and long duration of our light curves.

3 CROSS-CORRELATION ANALYSIS

3.1 Discrete correlation function

The typical method to determine time series correlation is the CCF. However, the CCF encounters problems when applied to unevenly sampled data, measurements with errors, or time series of different lengths (Alexander 1997). There are several robust methods that can correlate time series which can accommodate the conditions described above including the interpolated cross-correlation function (ICCF) (Gaskell & Peterson 1987), the DCF (Edelson & Krolik 1988), and the *z*-transformed discrete correlation function (ZDCF; Alexander 1997).

The DCF is a commonly used tool to probe for correlation in two time series that are unevenly sampled and for which the measurement errors are known. The DCF was developed by Edelson & Krolik (1988) to probe interband UV correlation in Akn 120 and NGC 4151. Since the inception of the DCF it has been used numerous times to probe for correlations between the X-ray and

UV mechanisms in AGN, for example Arèvalo et al. (2005), SV07, Marshall et al. (2008), and Gil-Merino et al. (2012).

The DCF is described fully by Edelson & Krolik (1988). The first step in calculating the DCF is to identify data pairs (X_i, Y_j) from each light curve that fall within the lag bin defined by $(\tau - \delta\tau/2) \leq \Delta t_{ji} < (\tau + \delta\tau/2)$, with $\Delta t_{ji} = t_j - t_i$, where τ is the transform in time (lag) and $\delta\tau$ is the bin width. The next step is to create a set of unbinned discrete correlation coefficients (UDCF$_{ij}$), for each data pair (X_i, Y_j),

$$\text{UDCF}_{ij} = \frac{(X_i - \bar{X})(Y_j - \bar{Y})}{\sqrt{(s_X - \bar{\sigma}_X^2)(s_Y - \bar{\sigma}_Y^2)}}, \tag{2}$$

where s_A is the variance and $\bar{\sigma}_A^2$ is the mean measurement uncertainty for the data sets and whose separation in time satisfies the condition above. Given M data pairs that fall within Δt_{ji}, the final step is to sum the UDCF and average over the number of data pairs,

$$\text{DCF}(\tau) = \frac{1}{M} \sum \text{UDCF}_{ij}. \tag{3}$$

An error on the discrete correlation coefficient may be calculated for each lag,

$$\sigma_{\text{DCF}}(\tau) = \frac{1}{M-1} \sqrt{\sum (\text{UDCF}_{ij} - \text{DCF}(\tau))^2}. \tag{4}$$

Only data that contribute to a given lag are used in the calculation of mean and variance. Edelson & Krolik (1988) acknowledge that binning the lag component does interpolate the correlation function but should not be confused with interpolation of data. With that in mind, consideration should be made to the lag bin width, $\delta\tau$, which is a compromise between accuracy in the statistical measurement of mean, uncertainty, and variance in equation (2) and resolution of the DCF, where the former demands larger $\delta\tau$, the latter requires small values of $\delta\tau$. While there is no standard rule for choosing lag bin width, $\delta\tau$, Edelson & Krolik (1988) argue that results depend weakly on bin width. A minimum value of $\delta\tau$ is dictated by the resolution of the coarsest time series.

3.2 Monte Carlo confidence intervals

In order to determine the confidence of the DCF, we generate 10^5 random X-ray light curves using the method described in Timmer & König (1995). We then apply the DCF with the real UV light curve and artificial X-ray light curves. The randomly generated X-ray light curves described in Timmer & König require a power-law slope, β, which relate power and frequency, $S(\omega) \sim \omega^{-\beta}$. Zoghbi et al. (2010) finds a power-law slope of $\beta \sim 0.77$ to central frequencies which we use in this work for the three X-ray energy bands.

Each artificial X-ray light curve is constructed without orbital gaps for an eight-day period to match the total observed length in each epoch. For each Monte Carlo simulation, two artificial light curves are generated, one for each epoch and each has a sampling rate to match the observed light curves in the respective epochs. Lastly, gaps are introduced into the artificial X-ray light curves by removing simulated data points that are approximately the same length as the commensurate gaps in the observed light curve.

The Monte Carlo simulations provide a distribution of 10^5 DCF coefficients at each lag interval. The DCF coefficients were not assumed to have a Gaussian distribution, so the mean and confidence intervals were not calculated using an arithmetic mean and a standard deviation. Instead we construct a cumulative distribution of the DCF coefficients and find the most probable, 95 and 99.9 per cent

coefficients which correspond to two sided *p*-values of 0.05 and 0.001, respectively (Fig. 2).

We note the difficulty in obtaining the slope of the power spectrum from the current data in either epoch given the uneven sampling. This work uses $\beta \sim 0.77$ of Zoghbi et al. (2010) but the power-law slope was not well constrained. The confidence intervals are sensitive to this estimate of slope and tend to be proportional to this value. For example, power-law slope of $\beta \sim 1.0$ produce confidence intervals larger than those displayed in Fig. 2.

3.3 Results

Four observed data pairs were tested with both epochs contributing to the combined light curves. The UV light curve was compared to the light curves in all three X-ray bands (UV–XRB, UV–XRS, and UV–XRI) (Fig. 2, top three panels). In addition, the blackbody and soft X-ray light curves were compared with the intermediate X-ray light curve (XRB–XRI, XRS–XRI) (Fig. 2, bottom two panels). Each DCF test used a lag bin width of $\delta\tau \sim 0.16$ d, and probed lags out to ± 7 d. Lag bin width, $\delta\tau$, is a compromise between resolution and statistical accuracy. A hard minimum limit of $\delta\tau$ is set by the time resolution of the light curves, ~ 0.05 d.

The asymmetries in the 95 and 99.9 per cent confidence intervals in Fig. 2 result from the uneven sampling rate, length, and gaps in the light curves. This causes varying numbers of data pairs to be found at each lag which reflect in the undulating shape of the confidence interval.

The UV–XRB, UV–XRS, and UV–XRI DCFs (top three panels in Fig. 2) exhibit similar features. There is a weak (~ 95 per cent confidence) anticorrelation found at ~ 5.3 d where the UV leads the X-ray bands. Additionally, there is a weak (~ 95 per cent confidence) correlation found at ~ 6.4 d again with UV leading the X-ray bands. The two bottom panels in Fig. 2 show a very strong peak at zero lag for the blackbody (XRB) and intermediate X-ray bands (XRI) (>99.9 per cent) and soft (XRS) and intermediate X-ray bands (XRI) (>99.9 per cent).

4 DISCUSSION

We have examined for time delays between the X-ray and UV light curves of 1H 0707–495 using the DCF. There were no notable lags detected between the UV and X-rays bands. The most significant features in the DCF were at the 95 per cent confidence level, consistent with the UV leading the X-ray fluctuations by ~ 5.3 and ~ 6.4 d. No features were detected at ~ 0.2 d, which corresponds to the light-travel time between the two regions assuming a standard thin accretion disc.

The ~ 6.4 d lag is seen as a correlation between the UV and X-ray bands. Such a lag could arise from Comptonization of UV photons in the corona, but this is unlikely for 1H 0707–495. First, the accretion disc emission attributed to the *UVW*1 band is only about 1/50 the value of the peak emission at $kT \approx 45 - 50$ eV (Vasudevan et al. 2011), therefore such a signature will be very weak. Secondly, analysis of the Fe K α emissivity profile suggests the corona in 1H 0707–495 is very compact with approximately 90 per cent of the power-law photons originating from $<15\,R_S$ during these observations (Wilkins et al. 2014). It is unlikely that significant Comptonization is taking place at such a large distance.

A UV lead could also result from a propagation scenario (Lyubarsky 1967), where fluctuations propagate in the disc first modulating the UV-emitting region and eventually reach the
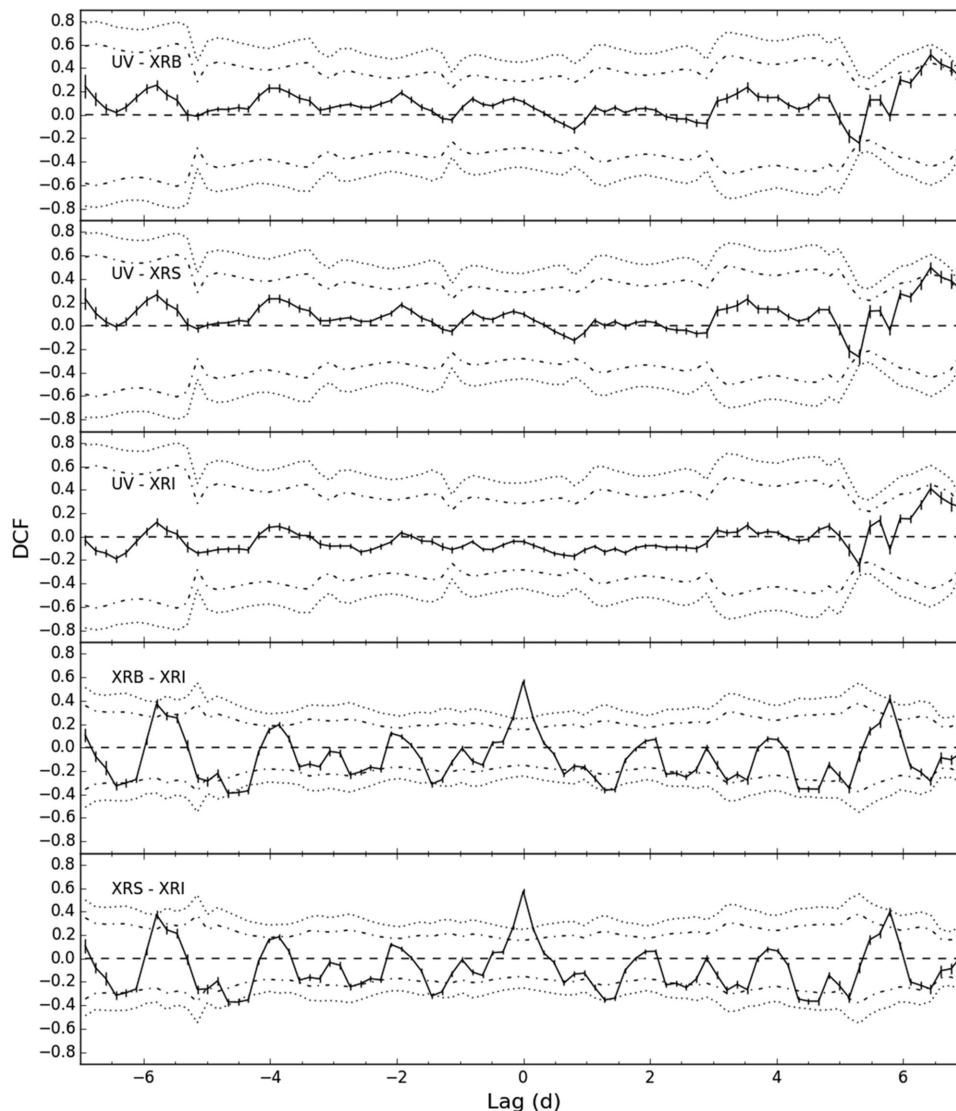
Figure 2. The DCF results of combined epoch light curves. The lags are relative to the first light curve listed in the plot (negative lags indicate the UV follow the X-rays). In all plots, the solid line indicates discrete correlation coefficients, the dashed line shows most probable value from Monte Carlo confidence tests while the dash–dotted and dotted lines indicated 95 and 99.9 per cent confidence intervals, respectively. Compared light curves are listed in each panel.

X-ray-emitting region at smaller radii. This also seems unlikely for 1H 0707–495. At $\sim$200 R_S, where we expect the *UVW*1 emission to originate from, we can estimate the inflow time-scale in a standard accretion disc from equation (5) of LaMassa et al. (2015). Assuming a viscosity parameter of 0.1 and that 1H 0707–495 hosts a Kerr black hole (i.e. radiative efficiency, $\eta = 0.3$) that is radiating at the Eddington luminosity (Zoghbi et al. 2010), the inflow time-scale would be several orders of magnitude larger than the observable time-scales.

Reprocessing of X-ray photons in the accretion disc could make the disc material hotter than if heated by accretion alone. If this emission is entirely absorbed and re-emitted, it should show the variability associated with the X-ray source. If the standard accretion disc around the black hole in 1H 0707–495 were being illuminated by an isotropically emitting source located at a height of 10 R_S above the disc, approximately 30 per cent additional flux would emerge in the *UVW*1 band than from the disc alone. If the X-ray source were located at 100 R_S, the additional flux in the *UVW*1 band would be approximately 40 per cent. Given these values are

significantly more than the $\sim$1 per cent variations we are observing in the *UVW*1 band indicates the X-ray source may be illuminating the disc anisotropically, which is consistent with the interpretation of a compact corona in 1H 0707–495.

The second feature in the DCF, of equally modest confidence to the $\sim$6.4 d lag, is an anticorrelation found between the UV and X-ray emission at a lag of approximately 5.3 d. We can speculate whether such an anticorrelation could arise in extreme gravitational environments like those present in 1H 07070–495. Given the centrally compact nature of the X-ray source gravitational light bending is significant. Depending on its height above the disc, the amount of radiation seen from an isotropic emitting source would look different for a distant observer and one at the disc (e.g. Miniutti & Fabian 2004).

Variability in the structure of the corona can also complicate the situation. As Wilkins et al. (2014) demonstrate the radial extent of the corona in 1H 0707–495 can vary by about 30 per cent. While the work of Wilkins et al. (2014) was based on flux-resolved spectra and did not constrain the variability time-scales, there are indications

from another NLS1, Mrk 335, that these variations could occur over the course of days (Wilkins & Gallo 2015).

A second possibility that could lead to the anticorrelation is if the primary X-ray source were moving at a significant velocity (e.g. if it were the base of a jet). In this case, beaming effects would modify the emission seen by the disc again making an intrinsically isotropic source appear anisotropic (e.g. Reynolds & Fabian 1997; Beloborodov 1999; Gallo et al. 2015). These arguments are simply conjecture, but could provide motivation for further investigation; however, given the modest significance of the feature we do not elaborate further.

The fact that we do not find any strong correlations between the UV and X-ray wavebands may not be surprising. We are confident that component dilution (i.e. multiple physical components contributing to emission in a given band) is present in the X-ray bands and this is likely also the case for the UV band. There is also the matter that the X-ray region is compact and light bending will significantly diminish the amount of X-ray light reaching the disc at $>100\,R_S$. An isotropically emitting corona extending over a large fraction of the disc would generate more significant correlations between the UV and X-ray light curves.

The correlation between the XRS–XRI bands at zero lag are consistent with Zoghbi et al. (2010) results finding an ∼30 s reverberation lag and ∼200 s lead between two similar bands (0.3–1.0 keV and 1.0–4.0 keV). We lack the resolution in the DCF to identify these lags separately in this study.

The blackbody (XRB) and intermediate (XRI) X-ray bands are also significantly correlated with zero lag. The blackbody component (see fig. 8 in Zoghbi et al. 2010) contributes most significantly in the XRB band. If this is thermal disc emission generated in the inner few gravitational radii of the disc, it could serve as the source of seed photons for Comptonization in the corona producing the strong correlation with the power-law-dominated XRI band. Alternatively, in the strong gravity regime close to the maximum spinning black hole returning radiation (Cunningham 1976) can heat the inner accretion disc. If this radiation penetrates the disc to an optical depth greater than 1, it will then reradiate as a blackbody. This can lead to a correlation between the power law and blackbody emission (i.e. XRI and XRB). Such behaviour was seen in the flux-resolved spectral analysis of a very similar NLS1 *IRAS* 13224–3809 (Chiang et al. 2015).

5 CONCLUSION

The results of our analysis do not reveal any strong correlations between the UV- and X-ray-emitting regions in the NLS1 1H 0707–495 on time-scales of less than a week. This may not be surprising in the case of 1H 0707–495 given its extremely compact X-ray-emitting region. In such cases, any correlations are expected to be weak. Long-duration observations with *XMM–Newton* (and *Swift*) have provided the opportunity to begin examining UV and X-ray timing studies on longer time-scales (e.g. weeks to months), but these observations require massive time investment. Dedicated multiband timing missions such as *Astro-Sat* will improve such investigations.

ACKNOWLEDGEMENTS

REFERENCES

Alexander T., 1997, in Maoz D., Sternberg A., Leibowitz E. M., eds, Astrophysics and Space Science Library, Vol. 218, Astronomical Time Series. Kluwer, Dordrecht, p. 163
Alston W. N., Vaughan S., Uttley P., 2013, MNRAS, 435, 1511
Arèvalo P., Papadakis I., Kuhlbrodt B., Brinkmann W., 2005, A&A, 430, 435
Beloborodov A. M., 1999, MNRAS, 510, 123
Boller T. et al., 2002, MNRAS, 329, L1
Breedt E. et al., 2009, MNRAS, 394, 427
Breedt E. et al., 2010, MNRAS, 403, 605
Cameron D. T., McHardy I., Dwelly T., Breedt E., Uttley P., Lira P., Arèvalo P., 2012, MNRAS, 422, 902
Chiang C-Y., Walton D. J., Fabian A. C., Wilkins D. R., Gallo L. C., 2015, MNRAS, 446, 759
Cunningham C., 1976, ApJ, 208, 534
Edelson R. A., Krolik J. H., 1988, ApJ, 333, 646
Fabian A. C., Ballantyne D. R., Merloni A., Vaughan S., Iwasawa K., Boller T., 2002, MNRAS, 331, L35
Fabian A. C., Miniutti G., Gallo L. C., Boller T., Tanaka Y., Vaughan S., Ross R. R., 2004, MNRAS, 353, 1071
Fabian A. C. et al., 2012, MNRAS, 419, 116
Gallo L. C., 2006, MNRAS, 368, 479
Gallo L. C., Tanaka Y., Boller T., Fabian A. C., Vaughan S., Brandt W. N., 2004, MNRAS, 353, 1064
Gallo L. C. et al., 2015, MNRAS, 446, 663
Gaskell M. C., Peterson B. M., 1987, ApJS, 65, 1
Gil-Merino R., Goicoechea L. J., Shalyapin V. N., Braga V. F., 2012, ApJ, 744, 47
LaMassa S. M. et al., 2015, ApJ, 800, 144
Leighly K. M., Moore J. R., 2004, ApJ, 611, 107
Lohfink A. M., Reynolds C. S., Vasudevan R., Mushotzky R. F., Miller N. A., 2014, ApJ, 788, 10
Lyubarsky Y., 1967, Int. J. Mod. Phys., D17
Markowitz A., Edelson R., Vaughan S., 2003, ApJ, 598, 935
Marshall K., Ryle W. T., Miller H. R., 2008, ApJ, 677, 880
Mason K. O. et al., 2001, A&A, 365, L36
Mason K. O. et al., 2002, ApJ, 580, L117
Miniutti G., Fabian A. C., 2004, MNRAS, 349, 1435
Nandra K., Clavel J., Edelson R. A., George I. M., Malkan M. A., Mushotzky R. F., Peterson B. M., Turner T. J., 1998, ApJ, 505, 594
Peterson B. M., 1997, An Introduction to Active Galactic Nuclei. Cambridge Univ. Press, Cambridge
Reynolds C. S., Fabian A. C., 1997, MNRAS, 290, 1
Shemmer O. et al., 2001, ApJ, 561, 162
Shemmer O., Uttley P., Netzer H., McHardy I. M., 2003, MNRAS, 343, 1341
Smith R., Vaughan S., 2007, MNRAS, 375, 1479 (SV07)
Tanaka Y., Boller T., Gallo L. C., Keil R., 2004, PASJ, 56, L9
Timmer J., König M., 1995, A&A, 300, 707
Vasudevan R., Gallo L. C., Robertson D., Fulford K., 2011, in Foschini L., Colpi M., Gallo L., Grupe D., Komossa S., Leighly K., Mathur S., eds, Proc. Workshop on Narrow-Line Seyfert 1 Galaxies and Their Place in the Universe. PoS(NLS1) 007
Wilkins D. R., Gallo L. C., 2015, MNRAS, 449, 129
Wilkins D. R., Kara E., Fabian A. C., Gallo L. C., 2014, MNRAS, 443, 2746
Zoghbi A., Fabian A. C., Uttley P., Miniutti G., Gallo L. C., Reynolds C. S., Miller J. M., Ponti G., 2010, MNRAS, 401, 2419

This paper has been typeset from a TEX/LATEX file prepared by the author.